Ship shadowing: model and data comparisons

William S. Helliwell and Gerald N. Sullivan

Arete Associates
P.O. Box 6024
Sherman Oaks, CA 91413

Burns Macdonald

Whitehead Associates
12012 Goshen Ave., #311
Los Angeles, CA 90049

Kenneth J. Voss

Physics Department
University of Miami
Coral Gables, FL 33124

ABSTRACT

The radiance distribution in a three dimensional volume of ocean water is obtained using a numerical finite difference scheme applied to the radiative transfer equation. The solutions to the model are obtained for a sunny sky and a surface ship that creates a shadow in the water. The model simulates the conditions for which data was collected. Radiance, upwelling and downwelling irradiance, water reflectively, and diffuse attenuation coefficient from the model and the experiment are compared.

1. INTRODUCTION

This paper, a comparison of theory and experiment in ocean steady-state radiative transfer, is based on measurements of radiance over 4π solid angles with instrumentation built by one of the authors (KJV), and on calculations of solutions of the radiative transfer equation which approximate the experimental conditions, by numerical methods developed by another of the authors (WSH). The radiance distributions are used to calculate vector irradiance distributions and apparent optical properties consisting of water reflectivity and diffuse attenuation coefficient. Using beam transmissometer measurements of the absorption coefficient and Gershun's Law, the absorption coefficient, which is an inherent optical

property, can be obtained from the data[1, 2, 3]. A different approach to obtaining the absorption coefficient is to adjust this quantity so that water reflectivity calculated from the model agrees with water reflectivity calculated from the data[4].

Shadowing due to ships or other objects, including the measuring instrument itself, greatly increases the complexity and scale of the light distribution problem. Previous work by Gordon[5] described shadow effects on irradiance for an instrument deployed from the side of a ship. This present paper goes much further and calculates the complete radiance distribution with shadow included.

Radiance distributions were measured in the geometry shown in Fig. 1. The instrument, an electro-optic radiance distribution camera system (RADS), was lowered off the stern of a ship and measurements were made at a number of depths ranging from 9 meters to 60 meters. RADS allows a complete spectral radiance distribution to be measured in a short period of time and the reduction of these data to absolute radiometric values is a routine procedure. Details of RADS have been given elsewhere[1,2,3]. Radiance measurements presented here have the sun off the ship's stern (1988 data), minimizing the effect of the ship's shadow, and also off the bow (1987 data) which maximizes the shadow effect.

The method of solution of the steady state radiative transfer equation in water has been developed for the radiance distribution (4π steradians) as a function of one space dimension- depth (1D) and for the radiance throughout an ocean volume (3D)[4,6,7]. This method uses various sky models and propagates the assumed input radiance through a smooth ocean surface and then through a chosen range of depths (1D) or throughout a volume of ocean (3D) using a given scattering phase function, an absorption coefficient, and a scattering coefficient, which all can vary with depth. Light scattering to all orders is calculated.

The 1D calculation models an ocean which does not change in the horizontal directions. The 3D method can model the radiance distribution which results when an underwater object perturbs the radiance field by absorption and reflection. This was used with a model of the ship's hull of Fig. 1 with parameter choices to match experimental conditions. The 3D results, together with the 1D, are compared with experimental values for radiance and irradiance profiles, and for diffuse attenuation coefficients and water reflectivities.

2. RADS MEASUREMENTS

The underwater spectral radiance distribution has been obtained using RADS. The heart of the system consists of two GE-2509 CID (charge-injection device) cameras. One camera points up to collect the hemisphere of down-welling radiance and the other points down to collect the up-welling radiance. The cameras have 260 x 253 pixels with low blooming. A Poynting 509 frame grabber converts the images to 8 bit digital data.

The digital data is sent to a computer on the ship via an RS-232 9600 baud link. A Hewlett Packard 310C microcomputer is used to control the camera system, display data, and store the data on a hard disc.

3. RADIATIVE TRANSFER

The radiance distribution L in a 3-dimensional scattering and absorbing medium satisfies the radiative transfer equation

$$\frac{dL}{ds} + c(\underline{x})\, L = \frac{b(\underline{x})}{4\pi} \int_{-\pi}^{\pi} \int_{0}^{\pi} p(\alpha)\, L(\underline{x},\phi',\theta') \sin\theta'\, d\theta' d\phi' \quad . \qquad (1)$$

Here, $\underline{x} = (x,y,z)$, z vertical, θ the polar zenith angle, and ϕ the azimuth angle. dL/ds is the directional derivative of L in the direction specified by (ϕ,θ). The function $c(\underline{x})$ is the attenuation coefficient, and $c(\underline{x}) = a(\underline{x}) + b(\underline{x})$, where $a(\underline{x})$ is the volume absorption coefficient and $b(\underline{x})$ is the volume scattering coefficient. In Equation 1 we assume that any depth dependence in the volume scattering function can be factored out so that it is a product of $b(\underline{x})$ and the scattering phase function $p(\alpha)$. The scattering phase function here is only a function of the angle α between incident and scattered radiance directions, (ϕ,θ) and (ϕ',θ'), and is normalized so that its integral over 4π steradians solid angle is 4π. Any scattering phase function can be incorporated into the equation. The one we have used here is a curve fit to measurements reported by Petzold[8] taken at AUTEC.

This equation is solved in water using a finite difference method with an iterative technique because of the scattering term on the right side. A fuller discussion of the solution of equation 1 is given in reference 7. In order to obtain a solution in the region of interest $\{x_{min} \le x \le x_{max}, y_{min} \le y \le y_{max}, z_{min} \le z \le 0\}$ radiance for all directions into the region must be specified at the boundaries.

These boundary values, involving incoming radiance only, are obtained from the 1D radiative transfer equation for the

simpler problem where the radiance is uniform horizontally but still depends on depth and direction. At the surface (z = 0) the in-water downwelling radiance is calculated starting, in this paper, from a clear-sky radiance distribution, a Gaussian of 10° width, refracted through the (smooth) water surface. To this is added the upwelling in-water radiance that has been reflected from the surface. Since the upwelling radiance is not known beforehand the boundary downwelling radiance is coupled into the iteration scheme. The peak value, in the sun direction, is normalized to one. At the maximum depth plane (z_{min}) incoming radiance is found assuming a Lambertian reflection with reflectivity extrapolated from the water reflectivity of the neighboring depths. As at the surface the incoming radiance depends on the solution and so is incorporated into the iteration scheme.

The 1D solution is used as the initial-guess input to the 3D code. For accuracy in the 3D finite difference solution the x,y,z grid points should be no further apart than one scattering length, 1/b. A typical choice of points is given in Fig. 2. The ship position is indicated as is the point off the stern (■) from which the RADS camera system was lowered. Depth planes are at 2.5 meter spacing. The angular grid points should be close enough so that the solid angle integration in Equation 1 has the desired accuracy. The choice of grid points is shown in the polar plots of Fig. 3. The radius in the upwelling display represents zenith angles from 0° to 90° while in the downwelling display it represents angles from 180° to 90°. The azimuth angle goes in opposite directions so that if the plot is folded along a vertical line the two hemispheres will match up. This display convention is also used in subsequent radiance contour plots.

Since the 3D radiance entering the sides of the ocean volume is fixed by the 1D solution the boundaries must be far enough away from the embedded object, the ship's hull, so that its influence on the radiance near the boundaries is small. Experience with the model has shown that a distance of a couple of scattering lengths is sufficient.

Computer memory and time available to obtain a solution limits the actual number of points used in a 3D calculation. The solution time is directly proportional to the number of spatial grid points and to the square of the number of directions. External storage could have been used to permit larger array sizes but this has not been done. A solution with x,y,z grid sizes of 21, 33, 31, and with 132 direction values takes about 4-1/2 hours on an Alliant FX/4 with one CPU. By contrast, 1D solutions take a few seconds on the same machine, or about 20 minutes on an AT-type personal computer. In all cases it takes about ten iterations for the radiance values to converge to better than 0.1%.

Once the radiance distribution has been obtained, the apparent optical properties can be calculated. The up- and downwelling irradiances are given by

$$E_u = \int_{\Omega u} L \cos\theta \, d\Omega \qquad E_d = \int_{\Omega d} L \cos\theta \, d\Omega \quad . \tag{2}$$

where Ωu amd Ωd are the upper and lower hemispheres, respectively. The water irradiance reflectivity r_w is defined by the equation

$$r_w = \frac{E_u(\underline{x})}{E_d(\underline{x})} \tag{3}$$

while the diffuse attenuation coefficient K_d is given by

$$K_d = \frac{-1}{E_d(\underline{x})} \frac{dE_d(\underline{x})}{dz} \quad . \tag{4}$$

4. MODEL AND DATA COMPARISONS

Data used in the comparisons came from two sets of RADS data, one taken on April 14, 1987, about 13:00 PDT, with the sun off the bow (Fig. 1), and one taken on October 14, 1988, about 13:00 PST, with the sun off the stern. Locations for each were approximately the same, off San Clemente Island, California. In both cases the ship, the R/V R.G. Sproul, had its axis in the sun plane. The 1987 data is discussed in references 1 and 2, and the 1988 data in reference 3. Only a selection of depths is presented here.

The depth-dependent volumetric absorption and scattering coefficients used in the modeling were taken from experimental values. The values of the total attenuation coefficient, c, Table 1, were measured and the scattering coefficient, b, determined from estimated values of the scattering albedo b/c, 0.75 for 1987 data, 0.80 for 1988 data. The absorption coefficient, a, was determined from a = c - b. The ship is modeled with several plane surfaces with the waterline cross-section shown in Fig. 2, a shallow V bottom, and a keel depth

Table 1

Depth (m)	1987 Data c(500) [1/m]	1988 Data c(491) [1/m]
0	.183	.297
2	.186	.283
4	.196	.286
6	.193	.288
8	.193	.281
10	.199	.286
12	.191	.304
14	.188	.297
16	.191	.304
18	.188	.358
20	.193	.330
22	.186	.332
24	.188	.316
26	.196	.321
28	.222	.316
30	.258	.304
32	.261	.258
34	.264	.244
36	.271	.265
38	.282	.244
40	.282	.216
42	.271	.218
44	.264	.206
46	.235	.204
48	.196	.202
50	.149	.199
52	.136	.197
54	.126	.195
75	.087	.195

of 2.4 meters. The entire hull has a reflectivity of 10%.

Polar plots of the radiance measurements (at 500 nm wavelength) and the model results at the x,y location indicated by the mark in Fig. 2 for the two sets of data are given in Fig. 4 and 5. The radius from the center represents zenith angles, 0° to 90° for upwelling radiance, 180° to 90° for downwelling. The azimuthal angle has been chosen so that when the downwelling and upwelling plots are folded about a vertical axis located between them, their 90° radiance values will correspond, edge to edge. The plane of the sun is shown with a dashed line. A contour level separation of 2.5 dB was chosen, starting from the maximum radiance value for downwelling and the minimum value for upwelling.

Both measurements and model show reductions in radiance from the direction of the ship, more prominent at the shallower depths but also visible deeper. The measurements also show evidence for the RADS support cables. These linelike features in the contour plots point off-center because the camera was not centrally mounted. These cables were not modeled. The measured radiance is not quite symmetric about the ship shadow, implying that the ship axis is out of the sun-plane by a few degrees. The model results were obtained with the ship axis in the sun-plane, and so the contours are symmetric.

Given in Fig. 6 are plots in the sun plane (i.e. along the dotted lines of Figs. 4 and 5) of the 1D and 3D radiance calculations based on the 1987 and 1988 data. Downwelling radiance angles here are from 90° to 270° and upwelling from 0 to 90° and 270° to 360°. The differences in the 1D and 3D curves show the influence of the shadow of the ship.

A sun-plane comparison of the 3D radiance calculations with the 1987 and 1988 RADS data is given in Fig. 7. The data has been normalized so that the upwelling irradiance at the

camera location calculated from the data and from the 3D model agree at 30 m depth. At the shallower depths the downwelling radiance from the model has a narrower profile than the data. At greater depths the modeled profile is as broad as the data but has a lower peak. These differences in radiance details have implications on the apparent optical properties.

In general the ship shadow is modeled well. The smooth model curve goes through the rough data plot. For the 1987 data, when the camera was in the shadow, the shadow has a significant effect on the radiance level. For the 1988 data, the camera was not in the direct shadow, however, the ship hull can be "seen" in the data and the model.

Apparent optical properties are shown in Fig. 8, 9, 10. The differences between the model results and the data are due to the differences in the radiance distributions mentioned above. The effect of the shadow on the 1987 data is pronounced. In fact, the diffuse attenuation coefficient is negative from 10 to 20 m depth. Ten meter depth is very close to the to edge of the shadow at the camera location off the stern of the ship.

The modeled radiance is obtained throughout a three dimensional region of water. The apparent optical properties have also been calculated at all x,y,z grid locations. Selected portions of these functions of three variables are shown in Fig. 11 to 16 using contour plots. The contour plots illustrate the function value over a plane at a specific depth. In all plots the value obtained by the 1D model is used as a reference value. This is the value that would be obtained with no ship shadow. Contours of values at ± 5% and ± 10% from the reference value are drawn. Regions where all values are more than 10% over the 1D value are filled in with vertical lines, and regions where all values are more than 10% under the reference value are filled in with horizontal lines.

The diffuse attenuation coefficient and the water reflectivity are shown in Fig. 11 and 12 for the conditions of the 1987 experiment. The effect of the ship is obvious. For the three depths, 9.2 m, 30 m, 55 m, the instrument is in the region where the 3D value is more than 10% different from the 1D reference value. The ship influences the properties closer to the x = 0 value as the depth increases. This is as it should be due to the peak sun radiance direction.

Fig. 13 and 14 show similar results for the modeled conditions of the 1988 experiment. In this case the sun is off the stern and the ship shadow effects are toward the bow. The camera location is in the region where the 3D values are within ±5% of the 1D value at all depths.

The upwelling and downwelling irradiance values at 30m depth are shown in Fig. 15 for the 1987 conditions and Fig. 16 for the 1988 conditions. The ±5% and ±10% contours are with respect to the non shadow values obtained from the 1D model.

5. DISCUSSION

The model predictions are in excellent qualitative agreement with the measurements but the quantitative fit should be better. Disagreement lies principally in the calculated r_w's being too low and the radiance sun-plane profiles too narrow.

Attempts have been made to bring the model results for the water reflectivity into better agreement with the data. A non-linear least squares fitting method similar to that used in Ref. 4 was employed. The depth profile for b was varied while keeping c fixed to the Table 1 values until the calculated r_w agreed with the data at the six depths where it was available. Agreement to one percent required b to decrease by about 10% for the 1988 conditions. This doesn't sound like much. However, since a is much smaller than b, and a = c - b with c fixed, the relative change in a ranged from +30% to + 60%. Increasing the absorption by this amount forced the radiance to decrease too rapidly as a function of depth.

Different sky models were used, but even in the extreme case of a uniform sky with no sun component the water reflectivity went down by only 10%. That is, r_w went from around .050 to 0.045, whereas the data is around .030.

The only quantity that was not varied was the scattering phase function. The calculated water reflectivity curve as a function of depth is greater than and parallels the measured curve for the 1987 data. Since water reflectivity is proportional to backscattered light, then less backscattering would give lower reflectivity. Indeed, California coastal water does have less backscattering than Carribean AUTEC water. The ratio of the integral over the backward direction hemisphere of a nominal California phase function to the same integral of the AUTEC phase function used in this paper is .50, close to the factor needed to reduce the modeled r_w to the measured r_w. Adjusting the scattering phase function will be the focus of future work.

Even without absolute accuracy the 3D model results can be used qualitatively. The depth plots, Fig. 8, 9, 10 show whether or not the instrument is functioning consistently throughout an experiment. The contour plots of Figs. 11-16 can be used to estimate how far from a ship instruments must be deployed to obtain measurements unaffected by the ships shadow.

Conversely, with further refinement, the 3D model could be used to correct apparent optical properties such as K_d and r_w measured near a ship to standardized values.

6. REFERENCES

1. Kenneth J. Voss, "Radiance distribution measurements in coastal water," Ocean Optics IX (1988), SPIE 925, 56-66 (1988).

2. Kenneth J. Voss, "Electro-optic camera system for measurement of the underwater radiance distribution", Opt. Eng., 28, 241-247 (1989).

3. Kenneth J. Voss, "Use of the radiance distribution to measure the optical absorption coefficient in the ocean", Limnol. and Oceanogr., 34, 1618-1626 in press (1989).

4. W. S. Helliwell and S. D. Gasster, "Obtaining inherent water optical properties from apparent water optical properties," Ocean Optics IX (1988), SPIE 925, 14-21 (1988).

5. H. R. Gordon, "Ship perturbations of irradiance measurements at sea. 1: Monte Carlo simulations", Appl. Opt., 24, 4172-4182 (1985).

6. W. S. Helliwell, "Finite-difference solution to the radiative-transfer equation for in-water radiance, "J. Opt. Soc. Am., 2, 1325-1330 (1985).

7. W. S. Helliwell, G. Sullivan, B. Macdonald, and K. Voss, "A finite-difference discrete-ordinate solution to the three dimensional radiative transfer equation," J. of Transport Theory and Statistical Physics, to be published.

8. T. J. Petzold, "Volume scattering functions for selected ocean waters", Scripps Institution of Oceanography Visibility Laboratory, SIO Ref. 72-78, October (1972).

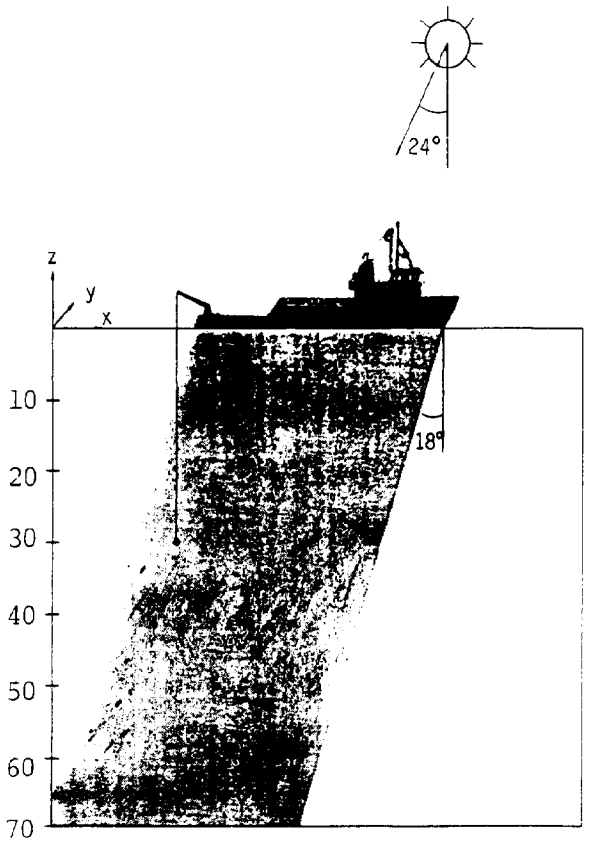

Fig. 1. Measurement geometry (1987 experiment). The ship axis is in the sun-plane. For the 1988 data the sun was off the stern at 45° (in-water 32°)

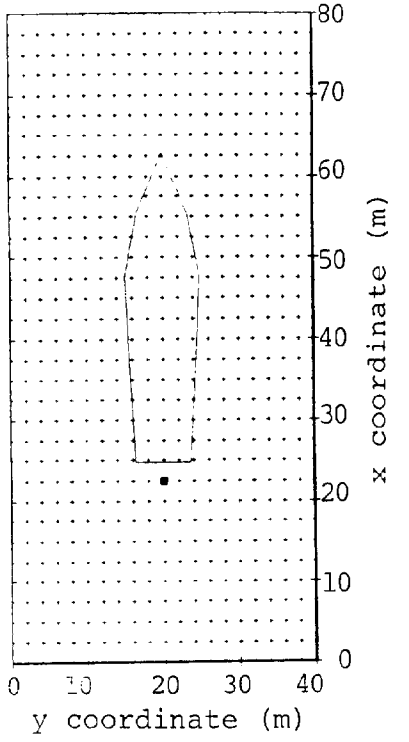

Fig. 2. Horizontal grid distribution showing ship and camera system (■)

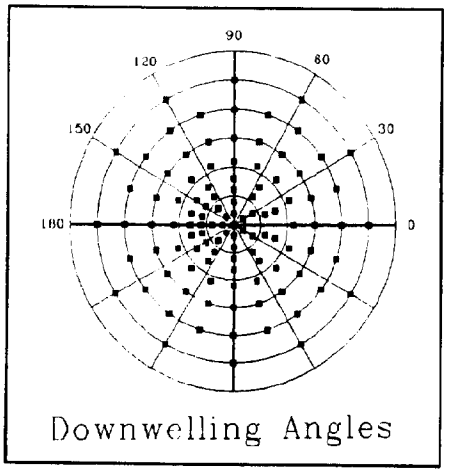

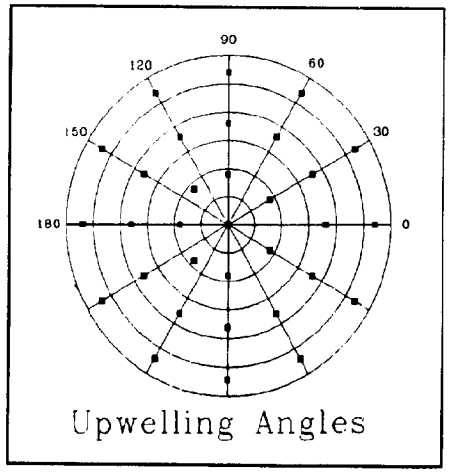

Fig. 3. Direction grid distribution

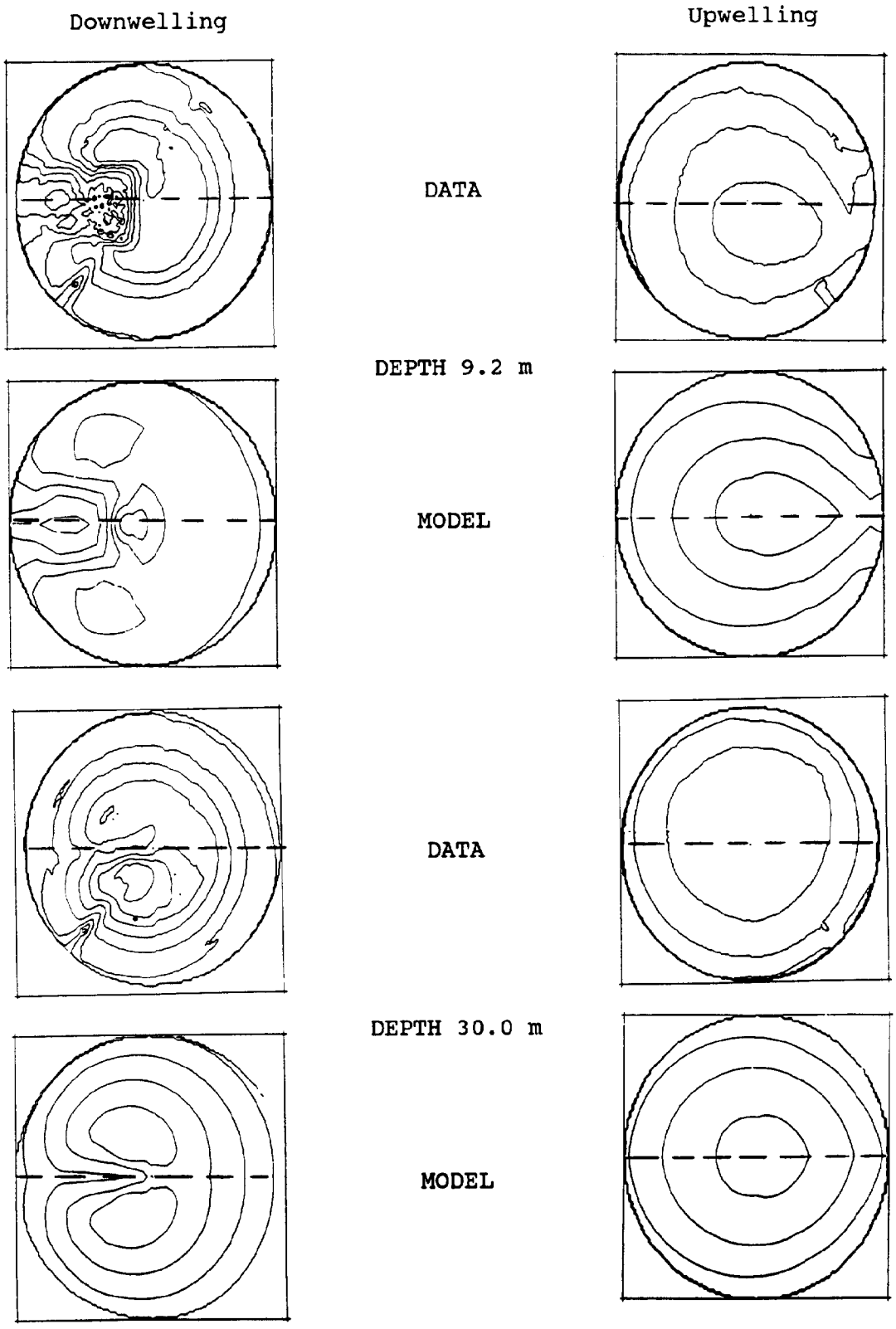

Figure 4. Contour levels of 1987 data and model

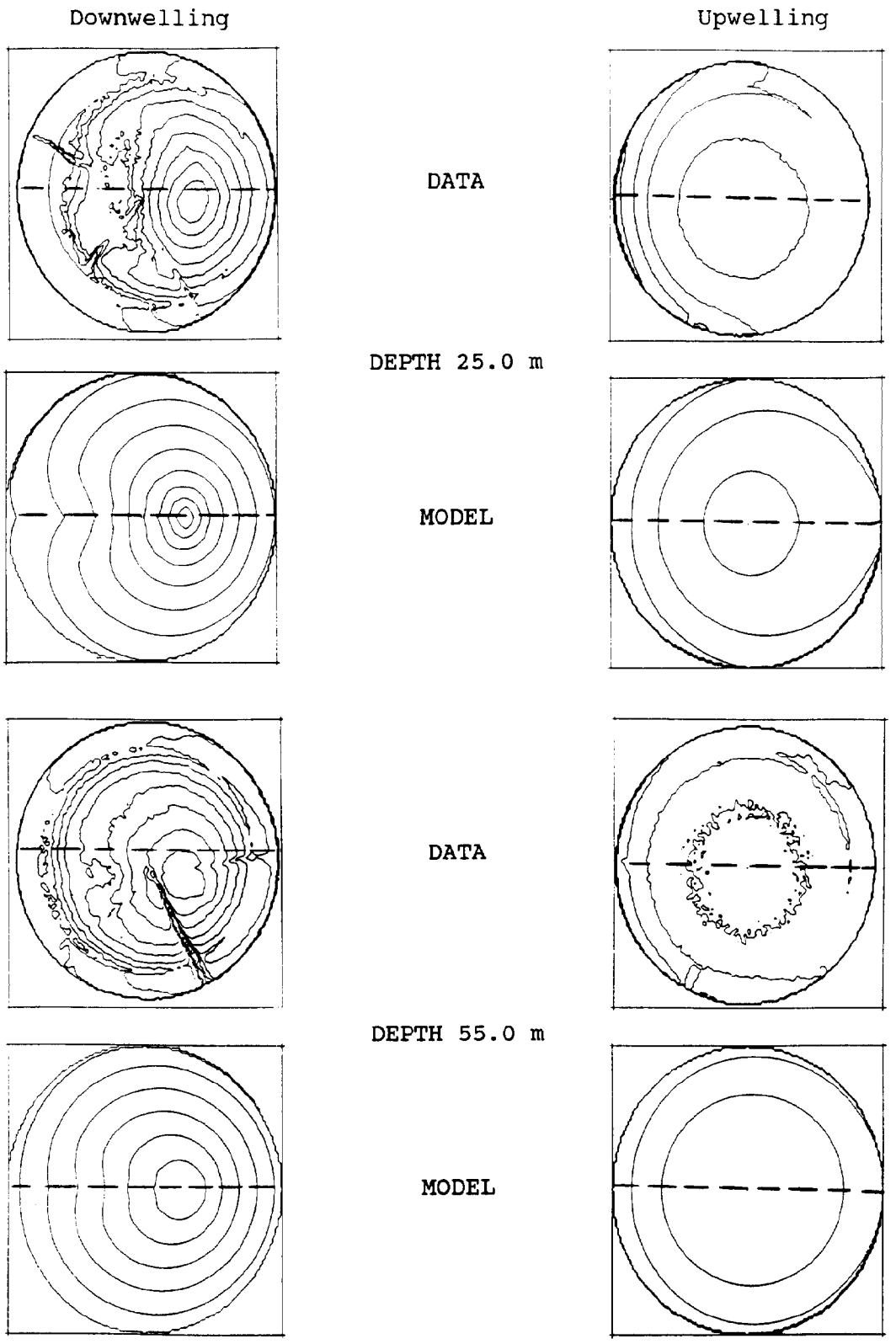

Figure 5. Contour levels of 1988 data and model

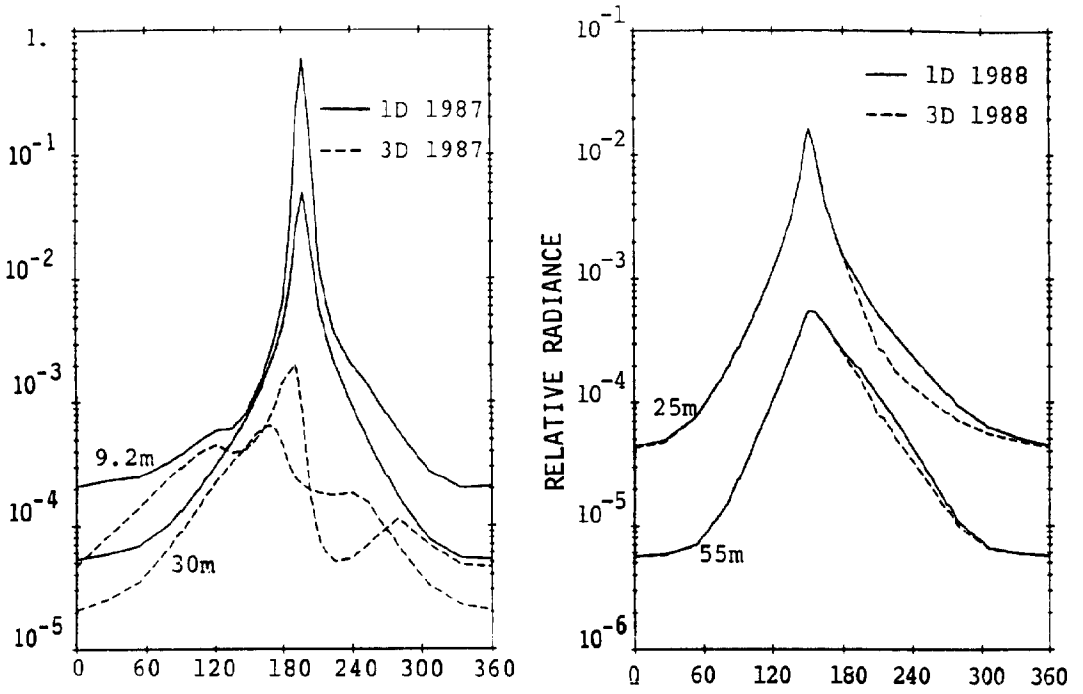

Figure 6. Sun-plane plot comparison of 1D and 3D models for 1987 and 1988.

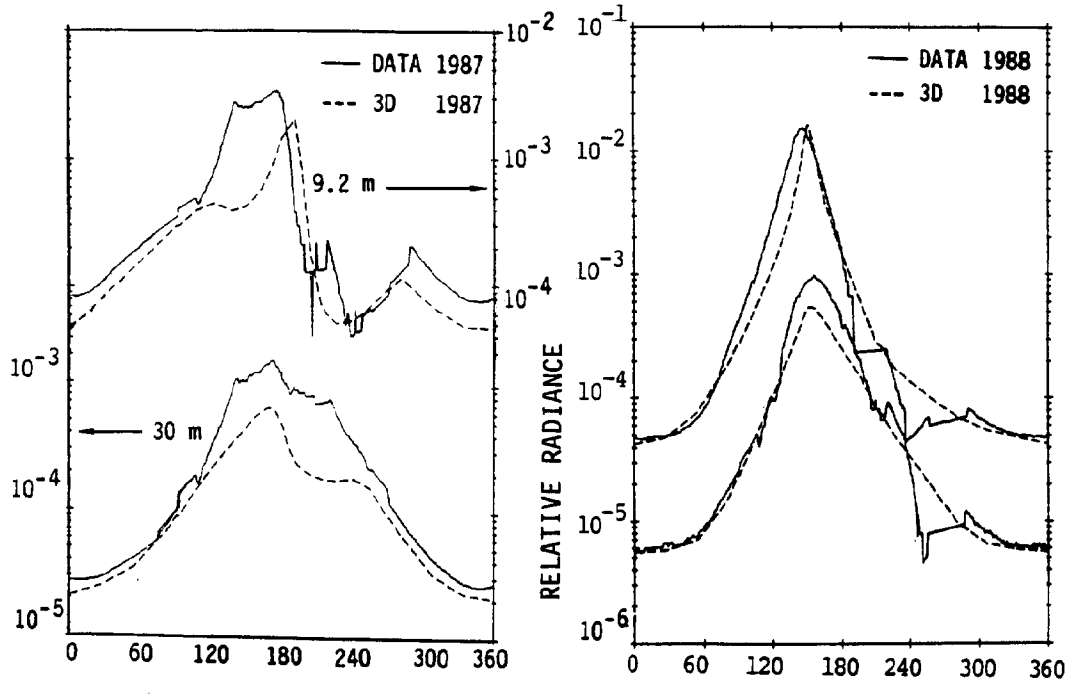

Figure 7. Sunplane plot comparison of data and 3D models for 1987 and 1988.

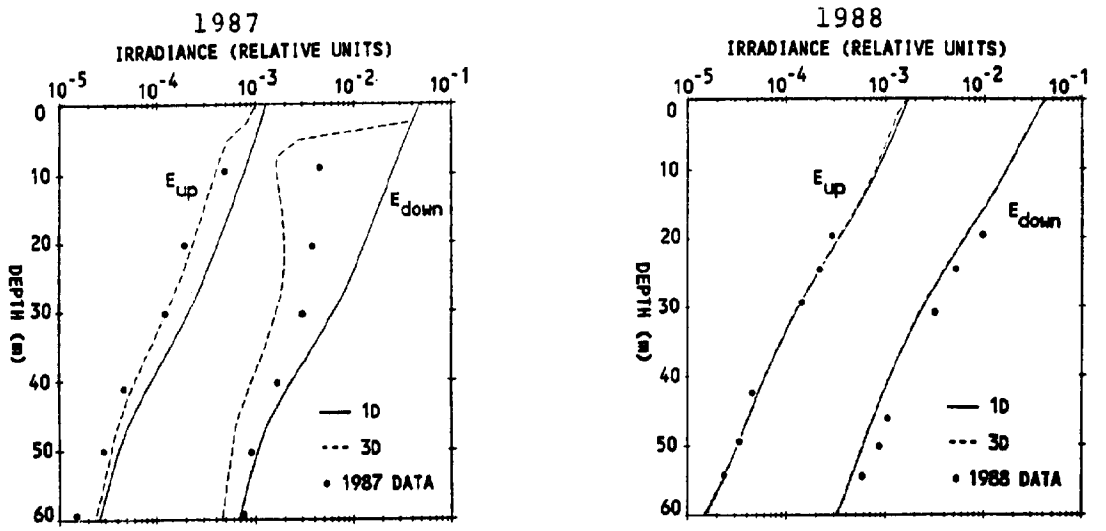

Figure 8. Irradiance versus depth

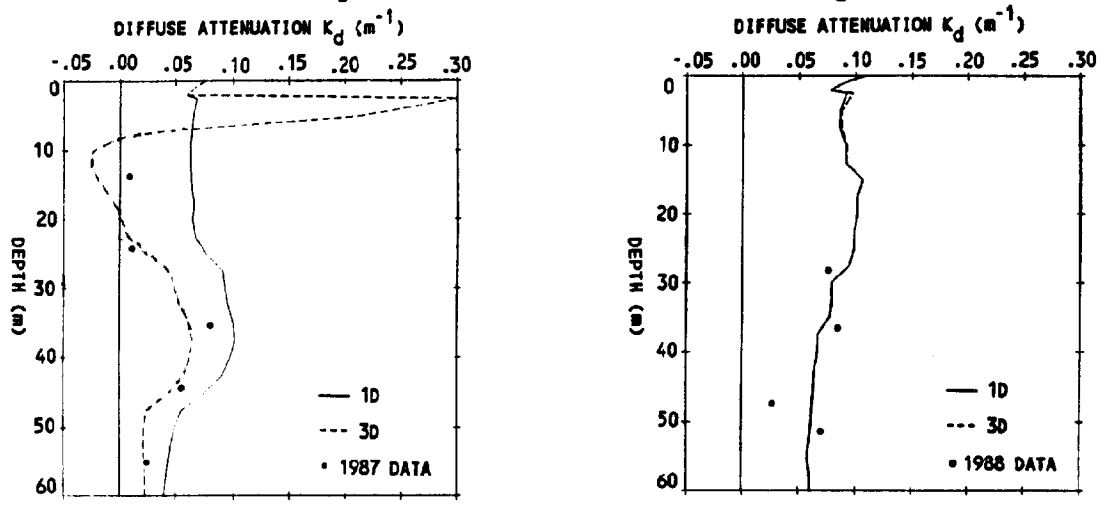

Figure 9. Diffuse attenuation versus depth

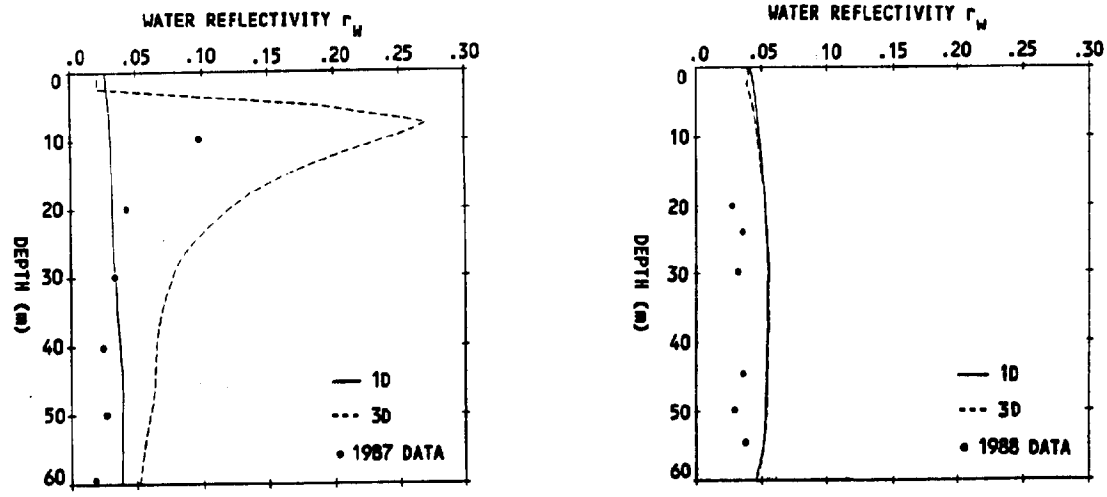

Figure 10. Water reflectivity versus depth

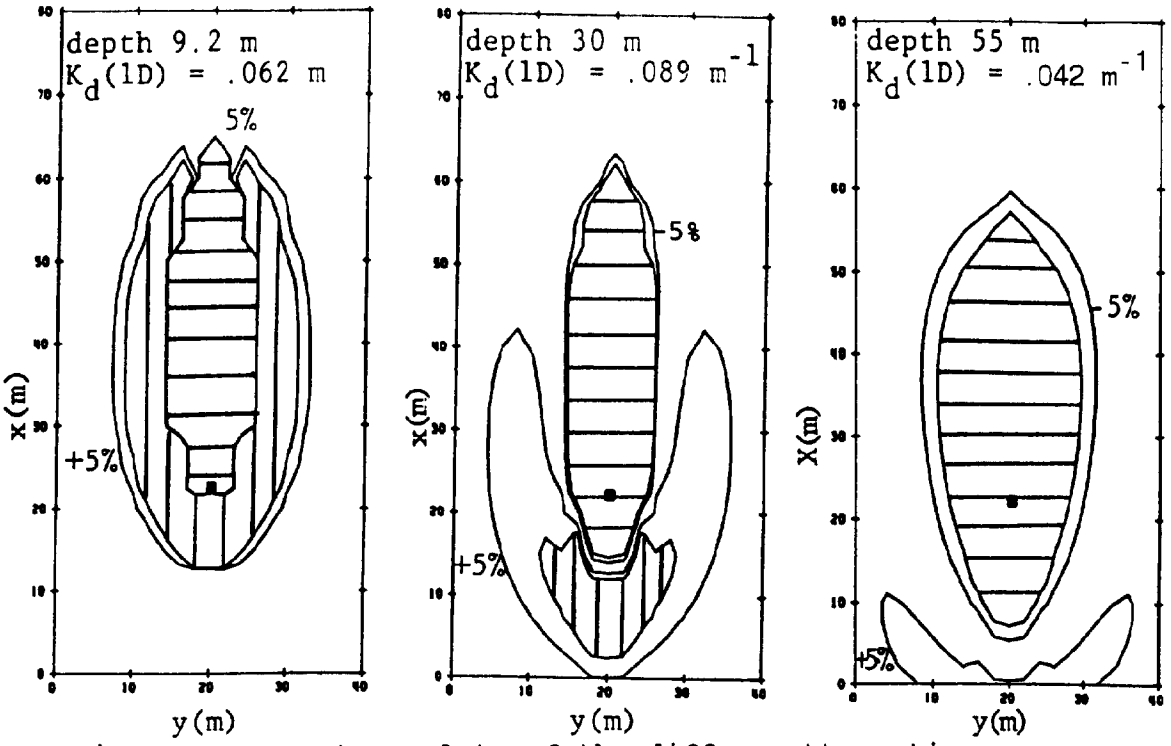

Figure 11. Contour plots of the diffuse attenuation coefficient K_d, from the modeled 1987 conditions.

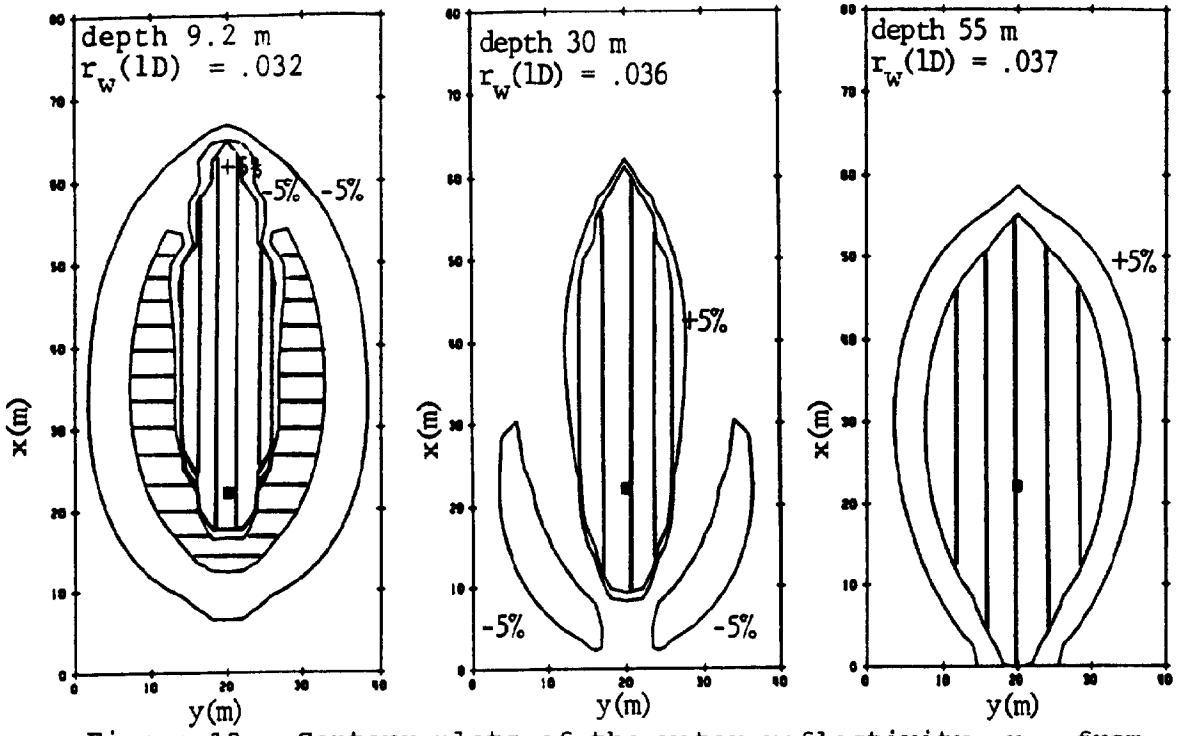

Figure 12. Contour plots of the water reflectivity, r_w, from the modeled 1987 conditions.

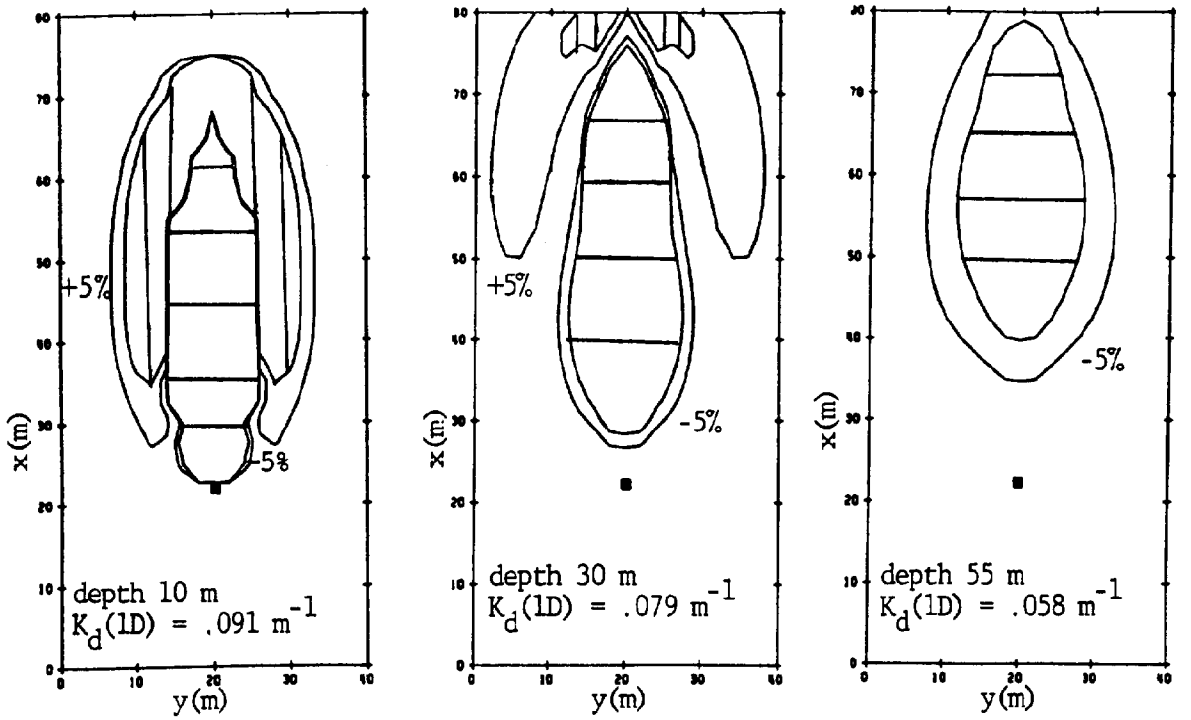

Fig. 13. Contour plots of the diffuse attenuation coefficient, K_d, from the modeled 1988 conditions.

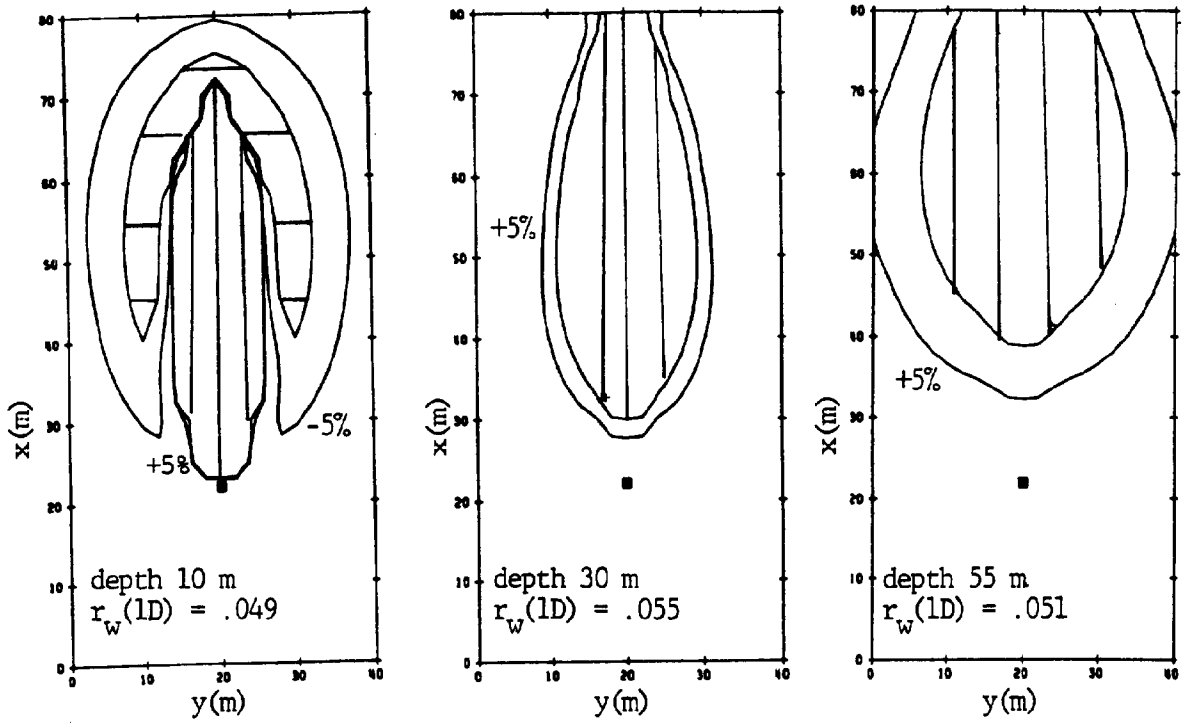

Fig. 14. Contour plots of the water reflectivity, r_w, from the modeled 1988 conditions.

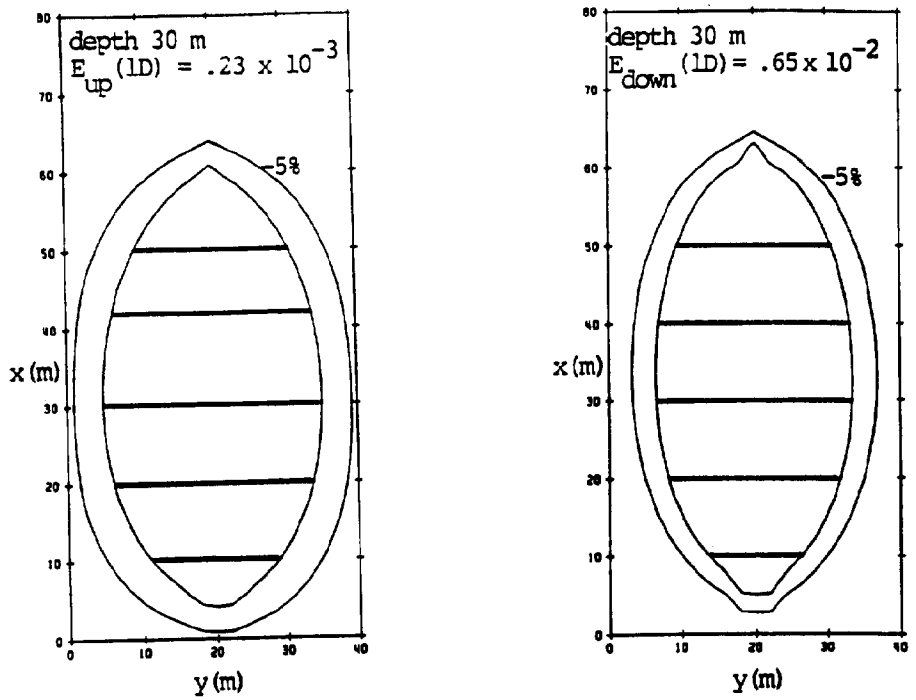

Fig. 15. Contour plots of upwelling, E_{up}, and downwelling, E_{down}, irradiance from the modeled 1987 conditions.

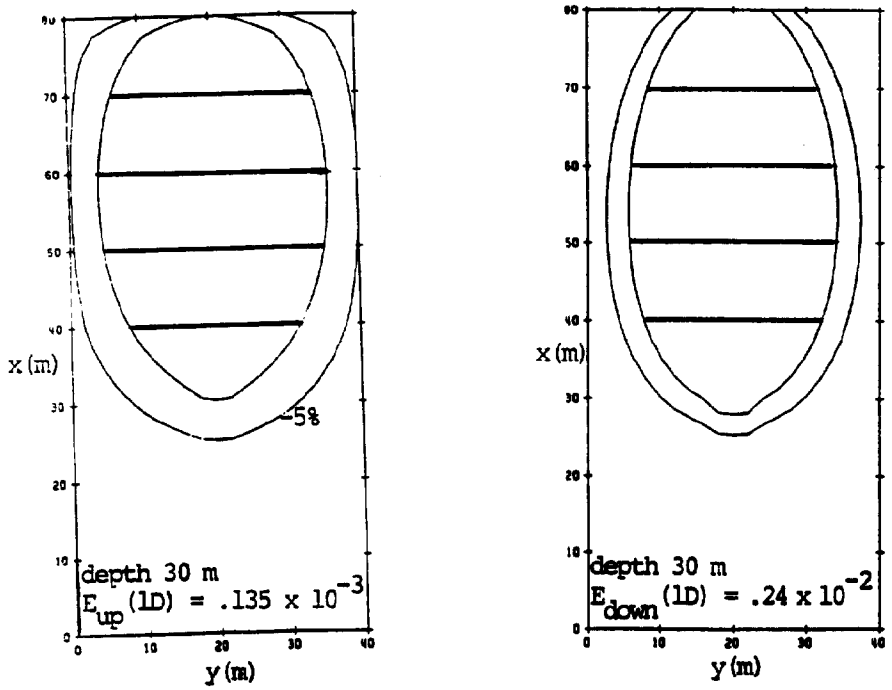

Fig. 16. Contour plots of upwelling, E_{up}, and downwelling, E_{down}, irradiance from the modeled 1988 conditions.